Towards Biofidelity Assessment of Upper Extremity of a 50th Percentile Male Finite Element Human Body Model

Ramakrishnan Balaji Iyer, Ayush P. Mehta, Amanda Hederskog, Christer Lundgren, Bronislaw Gepner, Jason L. Forman

Abstract Prediction of upper extremity injuries in motor vehicle collisions (MVCs) using human body model (HBM) simulations depends on the biofidelity of the model. This study combines findings from field data and model evaluation to assess current HBM performance. Injury distributions for AIS2+ upper extremity injuries among belted drivers and right front passengers in single-event crashes were first characterised using unweighted CISS data (2017–2022), identifying the most frequently injured upper extremity regions. Based on these findings, five representative loading scenarios were selected: clavicle axial compression, clavicle three-point bending, wrist compression with fixed and free elbow boundary conditions, and forearm three-point bending Finite element simulations were configured to replicate established post-mortem human subject (PMHS) test set-ups, including boundary conditions, loading directions, and constraints, for the given loading scenarios. The upper extremity responses of the THUMS v4.1 50th percentile male and the SAFER v.11.1 50th percentile male HBMs were then evaluated qualitatively through comparison with available PMHS experimental data. Overall, both HBMs reproduced experimental trends and relative stiffness characteristics in an acceptable manner, while revealing specific components and joints where further refinement is needed to improve upper extremity injury prediction in MVC simulations.

Keywords Clavicle, Wrist joint, Forearm, PMHS, Finite Element Human body Model.

I. INTRODUCTION

Upper extremity injuries are among the most common injuries in modern vehicles [1], and are one of the injury types for which females have been observed to be at greater risk compared to males [2]. The majority of AIS2+ upper extremity injuries in motor vehicle collisions (MVCs) are fractures. As with many other fracture types, upper extremity injuries can lead to considerable loss in long-term health-related quality of life, including pain and discomfort, ability for self-care, and limitations on function in one's everyday activities [3]. AIS2 upper extremity injuries have been reported to carry a 35% risk of at least some degree of permanent medical impairment [4]. Much has been written about the prevalence of upper extremity injuries in side impact, motivated primarily from a concern of shoulder loading during interaction with an intruding door [5-8]. However, as shown in recent field data studies, upper extremity injuries are also among the most common injuries occurring in frontal impact [1-2]. Many studies investigating upper extremity injury causation in frontal impact have focused on the potential for injury through interaction with a deploying driver airbag [9-12]. Aside from those airbag interaction studies, few studies have sought to investigate potential upper extremity injury mechanisms in frontal collisions [13-15]. Upper extremity injuries are not solely of concern for drivers, but also occur with similar frequency and injury patterns in right front passengers. As a result, unless they are addressed, they are very likely to persist in automated vehicles where all occupants are passengers.

Human body models (HBMs) provide a powerful computational framework for injury biomechanics research, enabling detailed evaluation of bone fracture risk and soft-tissue and ligament-level responses under controlled loading scenarios. As these models continue to advance in anatomical resolution and constitutive modelling, they have increasing potential to complement and, in some applications, augment traditional experimental and regulatory safety assessment methods. For HBMs to provide reliable injury predictions, they must demonstrate anatomical accuracy, numerical robustness, and biofidelity. Rigorous validation is therefore essential to ensure that model responses accurately reproduce human mechanical behaviour. Such validation is typically performed at multiple hierarchical levels, including isolated bone tests, joint-level loading conditions, and full-body impact configurations, often through comparison with post-mortem human subject (PMHS) experimental data.

R. B. Iyer (e-mail: zdf5ks@virginia.edu; tel: +1-434-257-3722) is a Research Engineer, A. Mehta is a Graduate Research Assistant, B. Gepner is a Research Assistant Professor and J. Forman is an Associate Professor at the Centre for Applied Biomechanics at the University of Virginia, USA. A. Hederskog and C. Lundgren are Senior Research Engineers at Autoliv.

The Total Human Model for Safety (THUMS) and SAFER M50 are high-resolution finite element (FE) HBMs developed with detailed anatomical representation and have undergone validation across several body regions, including the head, neck, thorax, abdomen, pelvis, and lower extremities. The THUMS v4.1 M50 upper extremity comprises the clavicle, humerus, radius, ulna, and the wrist joint includes the pisiform, triquetrum, lunate, and scaphoid interconnected through anatomically defined ligamentous structures. Within the currently published and free downloadable THUMS v4.1 M50 validation suite, upper extremity evaluation has primarily been limited to quasi-static lateral three-point bending and dynamic lateral compression of the humerus [16]. Comprehensive assessment of other critical anatomical regions, such as the clavicle, forearm, and wrist joint, has not yet been systematically reported. The SAFER M50 v.11.1 (made available to Autoliv for this project) upper extremity comprises the clavicle, humerus, radius, ulna, and the wrist joint includes the pisiform, triquetrum, lunate, and scaphoid interconnected through anatomically defined ligamentous structures. According to [17], validation of the SAFER HBM v.11.1 clavicle in axial compression and three-point bending has been performed, but these validation results have not been published. In addition, the SAFER HBM humerus has been validated. For the forearm, wrist and hand, validation remains unreported.

Given the diverse loading pathways responsible for upper extremity injuries in MVCs, including axial compression, bending, and joint-mediated load transfer, broader assessment of these anatomical components is required. A systematic evaluation of biofidelity and injury risk prediction under representative loading conditions is necessary to reproduce experimentally observed stiffness characteristics and load-transfer mechanisms relevant to injury prediction. However, biofidelity reference data for the upper extremities is limited to a few studies, some of which report limited information or sample sizes. Accordingly, this study does not seek to perform a full and final biofidelity assessment of HBM upper extremities, as the data to do so remain limited. Instead, this study seeks to take a preliminary look at the response of the SAFER M50 and THUMS M50 upper extremities under select load cases to examine their current state, and to identify what other reference information or assessments may be needed for biofidelity and injury assessment evaluation. To guide this, this study also presents a field data analysis involving AIS2+ upper extremity injuries for drivers and right front passengers in the CISS 2017–2022 dataset to highlight load cases important for upper extremity injury evaluation. Five representative loading scenarios were implemented: clavicle axial compression, clavicle three-point bending, wrist compression with fixed and free elbow boundary conditions, and supinated forearm three-point bending. These configurations were selected to evaluate both component-level and joint-level mechanical behaviour under loading modes relevant to MVC environments.

II. METHODS

Priorities based on Upper Extremity Injuries in the Field

The upper extremity is a complex body region with many different anatomical structures and potential injury types. To guide prioritisation for HBMs, our first step was to perform a basic examination of the types of upper extremity injury that occur in the field. For this, we examined AIS2+ upper extremity injuries in NHTSA's CISS database (collection years 2017–2022). We examined data from planar collisions with belted occupants, focusing on single-event crashes. Table I summarises the distribution of AIS2+ upper extremity injury cases in this dataset. The proportions of injuries by anatomical region were highly comparable between seating positions, with wrist injuries representing the most frequent region for both drivers and passengers (38.5% and 39.0%, respectively), followed by shoulder and clavicle (27.1% vs 24.4%) and the forearm (22.5% vs 19.5%), while injuries to the upper arm, elbow, hand/finger, and other upper extremity regions occurred at lower but similarly distributed rates. These results indicate that upper extremity injuries are not only as prevalent among drivers but also have similar dominance for right front passengers and exhibit closely matched regional injury patterns, despite differences in restraint geometry, steering-wheel presence, and expected occupant kinematics.

Thus, upper extremity trauma in frontal crashes cannot be attributed solely to driver-specific interfaces such as the steering wheel and driver airbag; instead, comparable injury patterns arise even in seating positions where these components are absent, suggesting that other vehicle interior structures and global loading environments also play important roles. Guided by the predominance of shoulder/clavicle, forearm, and wrist injuries in the field data, the subsequent literature review concentrated on post-mortem human subject (PMHS) experiments involving these anatomical regions.

TABLE I
DISTRIBUTION OF AIS2+ UPPER EXTREMITY INJURIES FOR BELTED DRIVERS AND RIGHT FRONT PASSENGERS IN SINGLE EVENT COLLISIONS (CISS 2017–2022, UNWEIGHTED)

Injury region	*Driver*	*Passenger*
Shoulder & Clavicle	27.1%	24.4%
Upper Arm	6.0%	9.8%
Elbow	7.3%	12.2%
Forearm	22.5%	19.5%
Wrist	38.5%	39.0%
Hand/Finger	16.1%	12.2%
UX Other	3.2%	7.3%

Based on the available experimental evidence and relevance to crash loading, four representative loading scenarios were selected, as shown in Table II, for model evaluation: clavicle axial compression, clavicle three-point bending, wrist compression with fixed elbow and free elbow boundary conditions, and supinated forearm three-point bending. These were selected based on a review of the available literature, seeking studies that may be of use in evaluating component-level upper extremity response for the high-frequency injury types shown in Table I – specifically, the clavicle (which comprised the majority of the shoulder & clavicle injury cases), the wrist, and the forearm. With a relative paucity of prior PMHS studies focused on the upper extremity, the literature review returned the following studies that contained sufficient detail for simulation (Table II). These formed the basis of our component simulations.

TABLE II
UPPER EXTREMITY EVALUATION CASES BASED ON THE FIELD DATA ANALYSIS AND AVAILABLE PMHS TEST RESULTS

Configuration	*Component / joint*	*Load case*	*Reference*	*Number of PMHS*
1	Clavicle	Axial compression	Zhang *et al.* 2014 [18]	10
2	Clavicle	Three-point bending		10
3(a)	Wrist joint, extension	Axial compression, free elbow	Forman *et al.* 2014 [19]	8
3(b)		Axial compression, fixed elbow		6
4	Forearm, supination	Three-point bending	Duma *et al.* 2002 [20]	5

Condition 1: Clavicle Axial Compression Test

Zhang *et al.* [18] conducted axial compression of the clavicle to replicate loading conditions representative of shoulder-belt interaction and direct lateral shoulder impacts in MVCs. These data provide force-based injury metrics that are particularly relevant for evaluating shoulder-belt loading in frontal impacts. Axial compression tests have demonstrated that clavicle fracture tolerance is sensitive to loading rate and boundary constraints, reinforcing the importance of replicating physiologic joint constraints in experimental configurations. Figure 1 shows the PMHS experimental set-up and the FE set-up.

In this study, 10 isolated clavicle specimens were potted at the sternal (medial) and/or acromial (lateral) ends and subjected to dynamic compressive loading along the anatomical axis of the clavicle. The actuator was displaced at 100 mm/s to a maximum displacement of 30 mm to ensure gross failure of the specimen and to achieve similar clavicle loading rate as measured in the side-impact sled test. Reported outcomes include peak failure force, impactor distance and reaction forces time history at the support plates. These test conditions were reconstructed in simulation. First, the left clavicle of the THUMS M50 was isolated from the pedestrian model. In the FE set-up, the mounting plates, support columns and the potting cups were modelled with hexahedral elements. The clavicle bone was then placed in the centre of the potting cups and connected to it via node to node. The rotation pin joints were defined by **CONSTRAINED_JOINT_REVOLUTE* between the potting cups and the column.

For the axial compression, one pin joint was used at medial end. The mounting plate was constrained in all degrees-of-freedom (DOF). The potting resin (similar to polyurethane resin - R1 FastCast®, Formula 891, Goldenwest Mfg., Cedar Ridge, CA) was assumed to be a linear elastic material with Young's modulus of 2.5 GPa. For the simulation, lateral end was translated in the medial–lateral direction at the experimental velocity, and no rotation or other translation was permitted. The force at the support plate in the vertical direction was recorded. The potting cup at the lateral end was moved along the clavicle axis and the force was plotted against the cup displacement

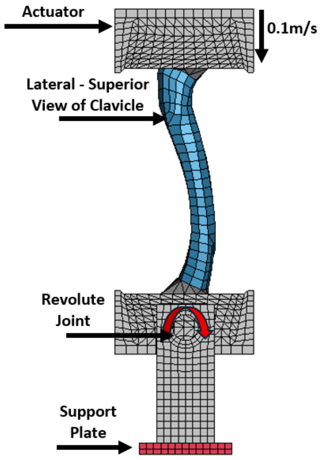

Fig. 1. Clavicle axial compression set-up: FE simulation set-up with THUMS M50 clavicle.

Condition 2: Clavicle Three-point Bend Test

Zhang *et al*. [18] conducted three-point bending tests of the clavicle to simulate transverse loading, such as that produced by belt edge loading or localised contact from interior structures [15]. In this configuration, the clavicle is supported at two outer points while a central actuator applies displacement-controlled or force-controlled loading at the midshaft. A 12.7 mm-diameter cylindrical section of aluminum loaded the clavicle midway along its length to failure; this loader was attached to the test machine actuator. The loader was displaced at 100 mm/s up to at least 60 mm to ensure gross failure of the specimen and to achieve similar clavicle loading rate as measured in the frontal impact sled test, as shown in Fig. 2. Outcome measures include force at fracture, displacement at failure, and structural stiffness. Fracture location most often occurs at the midshaft, corresponding to the region of maximum bending moment.

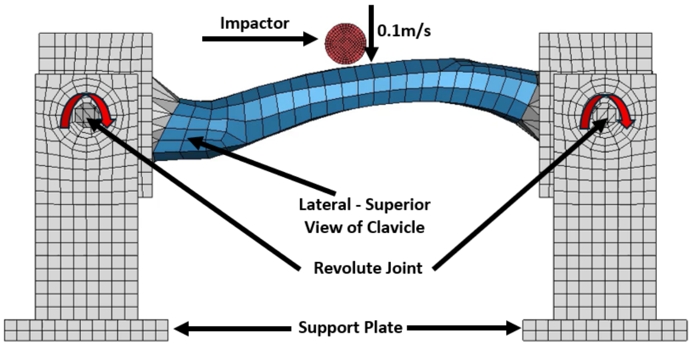

Fig. 2. Clavicle three-point bend test set-up: (a) PMHS experimental set-up [18] and (b) FE simulation set-up with THUMS M50 clavicle.

The FE model was created in a similar way as in axial compression test except for changing the boundary conditions and orienting the potting cups according to the experiment set-up. The rotation pin joints were defined between the potting cups and the column. For the three-point bending test, one pin joint was used at each extremity. The mounting plates were constrained in all directions using *BOUNDARY_SPC (single point constraint). The impactor was modelled as a cylinder of rigid material with aluminum properties, and its translation in the anterior–posterior direction (perpendicular to the clavicle longitudinal axis) was applied at the same rate as in the experiments. The potting resin was assumed to be a linear elastic material with Young's modulus of 293 MPa. The three-point bending FE model was then simulated using the clavicle material parameters in existing THUMS M50 model. Reaction forces in direction of loading, cortical bone strains, failure displacement and bone fracture locations were compared with the test data to investigate the influence of the material parameters on clavicle responses. For this test, the forces at two support plates were added to get the final force. With the boundary conditions defined, the three-point bending was simulated and the force–displacement graph was plotted along with test results.

Conditions 3 : Wrist Joint Axial Impact (Extended)

Forman *et al.* [19] investigated dynamic axial impact to the wrist joint of an outstretched hand to characterise wrist and distal forearm injury tolerance under crash-relevant loading. In that study, isolated male cadaveric forearm–hand complexes were tested using a drop-tower apparatus designed to simulate impact to an extended wrist. The specimens were positioned with the wrist extended to approximately 90°, and a guided impact mass was released to achieve an impact velocity of approximately 6 m/s, as shown in Fig. 3(a). To examine the influence of boundary conditions on load transmission and injury outcome, two elbow constraints were evaluated. In the fixed elbow configuration, the proximal nodes of the radius and ulna were rigidly constrained, whereas in the free elbow configuration, the mounting assembly was allowed to translate under inertial loading to better represent whole-body deceleration effects.

Fig. 3. Wrist joint axial impact set-up: FE simulation set-up for (a) extended, (b) instrumentation of THUMS M50 Wrist joint axial.

For the THUMS M50 simulations, the model was first repositioned to achieve approximately 90° wrist extension, consistent with the experimental configuration shown in Fig. 3(b). During repositioning of the wrist to achieve the required 90° flexion and extension postures, the forearm bones exhibited non-physical buckling due to excessive force transfer through the joint. To mitigate this numerical artifact, the forearm bones were temporarily rigidised during the repositioning process and subsequently restored to their deformable state for the simulations. Additionally, large rotations at the wrist joint led to ligament twisting and localised mesh distortion, resulting in poor element quality in certain regions. These issues were addressed through manual mesh correction, including localised node repositioning to restore acceptable element quality. A rigid impactor plate, representative of the experimental contactor, was then positioned above the flat palm. The mean acceleration time history derived from the PMHS experiments was prescribed to the rigid plate to drive the impact event. For the free elbow configuration, the elbow was constrained so that it could only move vertically and allow the forearm to respond dynamically under the applied loading. For the fixed elbow configuration, an additional rigid plate was introduced proximal to the elbow joint. The nodes associated with the elbow joint region were constrained to this plate to replicate the fixed boundary condition used in the PMHS tests. In the PMHS experiments, the elbow force time history was recorded. To ensure consistency in comparison, the elbow reaction force in the simulations was computed by extracting cross-sectional forces in the radius and ulna at the proximal forearm and summing the resultant force components to obtain the net elbow force response.

Condition 4: Supinated forearm Three-point Bend Test

Duma *et al.* [20] conducted a three-point bending of the forearm to simulate transverse loading conditions representative of bracing, contact with vehicle interiors, and interaction with restraint systems. In this configuration, the radius–ulna complex is supported proximally and distally while a transverse load is applied at the midspan, creating a controlled bending environment. A 9.48 kg impactor was dropped from a height of 2.0

m, producing a pre-impact velocity of approximately 4.42 m/s, as shown in Fig. 4(a). The impactor travelled along low-friction linear bearings to maintain precise alignment and high repeatability.

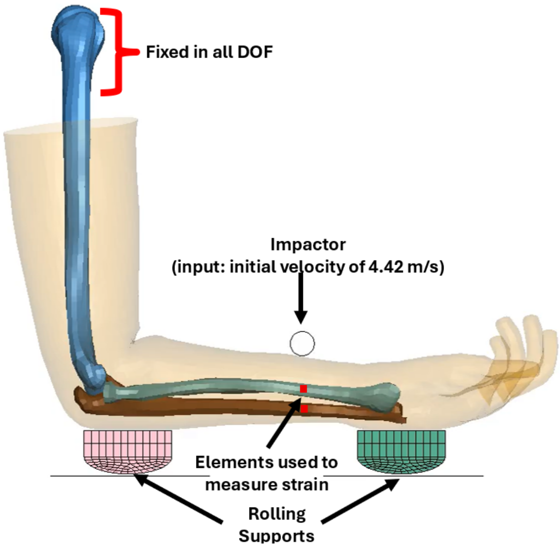

Fig. 4. Forearm three-point bend: (a) PMHS experimental set-up [20] and (b) FE simulation set-up for THUMS M50.

The FE set-up was constructed to replicate the PMHS three-point bending experiments using the THUMS M50 50th percentile male HBM. The right upper extremity was first positioned such that the elbow was flexed to 90°, forming a right angle between the upper arm and forearm, and the palm was rotated to face upward to achieve a supinated forearm posture. The right upper extremity was then isolated at the shoulder and used as a standalone segment for the forearm three-point bending simulations.

To reproduce the experimental boundary conditions, the forearm was supported proximally and distally using kinematic constraints analogous to roller supports. Specifically, translationally constrained supports were placed beneath the elbow and wrist joints, and a rigid plate, fixed in all DOF, was positioned beneath both supports to provide a stable foundation. In addition, the shoulder was constrained by fully fixing the proximal end of the humerus in all DOF, thereby stabilising the upper arm while allowing bending of the forearm between the two supports, as shown in Fig. 4(b).

The impactor was modelled as a rigid body with a mass of 9.48 kg and a cylindrical contact interface with a diameter of 12 mm. It was positioned at a location corresponding to two-thirds of the distance from the olecranon, matching the distal-third impact site used in the experiments. An initial velocity of 4.42 m/s was prescribed to the impactor to reproduce the target impact severity and strain rate conditions.

Model instrumentation was designed to capture global and local response measures consistent with experimental data. To quantify local bone response, strain was extracted from cortical bone elements of the radius and ulna in the region immediately under the impact site. These outputs provided direct FE analogs to the experimental force and strain gauge measurements, enabling detailed comparison of global structural behaviour and local bone strain between simulations and physical tests.

SAFER HBM

All load cases, i.e. clavicle axial compression, clavicle three-point bending, wrist and distal forearm compression with both fixed elbow and free elbow boundary conditions, and supinated forearm three-point bending, were also implemented in the SAFER M50 HBM using an analogous upper extremity configuration. To facilitate direct examination of model performance, the SAFER M50 simulations employed the same geometric set-up, boundary conditions, and loading configurations as those defined for the THUMS M50 model. As with THUMS M50, SAFER M50 experienced issues during repositioning, requiring manual modifications: when positioning the wrist in an extended and flexed position, the carpal bones moved to the side of the radius and ulna. To solve this, the position of the hand and carpal bones were manually positioned over the radius and ulna. This parallel implementation enabled assessment of upper extremity responses across two different 50th percentile male HBMs under a common set of representative loading scenarios.

III. RESULTS

The component response of the THUMS AM50 and SAFER M50 model was examined by comparison with matched PMHS responses. All the simulations were performed in LS Dyna™ R14.0 solver. By closely reconstructing the boundary conditions, impact severity, and measurement locations between simulations and experiments, the numerical results were used to examine the current state of the THUMS AM50 and SAFER M50 upper extremity components relative to the PMHS responses.

Condition 1: Clavicle Axial Compression Test

This figure presents the clavicle axial compression force–displacement response of the THUMS M50 model relative to the experimental PMHS corridors. Force (N) is plotted on the vertical axis and actuator displacement (mm) on the horizontal axis. Figure 5(a) shows the force vs displacement plot for THUMS M50 and SAFER M50 compared against PMHS test results. The PMHS clavicle axial compression tests exhibited an average peak force of approximately 3400 N at a displacement of about 7–8 mm, with the experimental corridor spanning roughly 2500 N at the lower boundary to 4200 N at the upper boundary. In contrast, the THUMS M50 and SAFER M50 simulation reached a higher peak force of around 3650 N and 2500 N at a smaller displacement of roughly 2–3 mm, respectively, and then maintained elevated force levels over the subsequent displacement range.

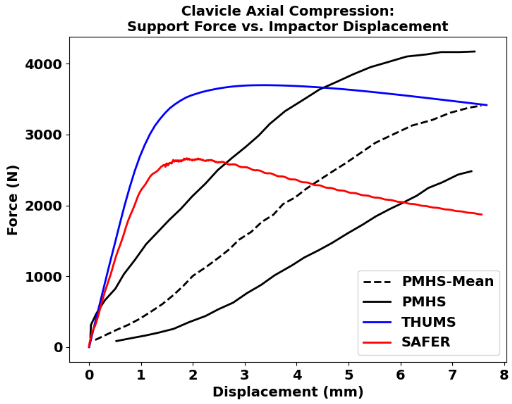

(a)

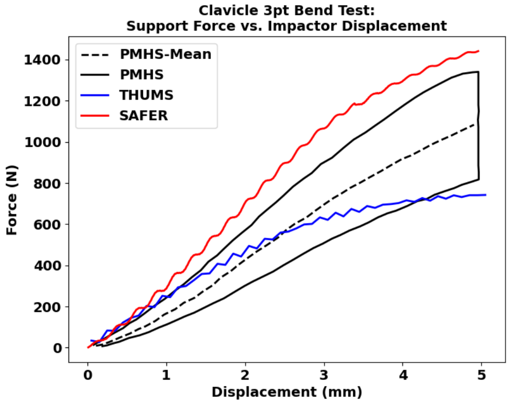

(b)

Fig. 5. Clavicle: (a) axial compression, and (b) three-point bending simulation results. Reaction forces from the support plate vs displacement of the impactor. THUMS M50 (blue), SAFER M50 (red), compared to the PMHS corridor [18] (black).

Condition 2: Clavicle Three-point Bend Test

Figure 5(b) shows the clavicle three-point bending force–displacement response for the THUMS M50 and SAFER M50 plotted against the experimental PMHS response corridors. The experimental force corridor ranged from roughly 750 N at the lower boundary to 1100 N at the upper boundary. The peak forces recorded in the THUMS M50 and SAFER M50 were about 700 N and 1400N, respectively, at 5 mm of displacement.

Condition 3a: Extended Wrist Joint (Free Elbow)

Figure 6(a) and 6(b) show the time history of axial elbow force (Fz) for the free and fixed elbow wrist loading cases, respectively, comparing THUMS M50 to the PMHS corridor. The solid dark curve is the PMHS mean response, with dashed curves indicating ±1 standard deviation, while the green curve represents the THUMS M50 simulation. In the free elbow case, the PMHS mean elbow axial force reaches a maximum compressive peak force of approximately −4300 N to −4400 N, while the THUMS M50 curve attains a peak force of about −3500 N and for SAFER M50, the peak force was −3550 N.

In the fixed elbow case, the PMHS mean elbow axial force reaches a maximum compressive peak of approximately −5200 to −5400 N, while the corridor spans from about −4800 N at the upper boundary to roughly −6000 N at the lower boundary. The THUMS M50 curve attains a similar peak force of around −5700N and SAFER M50 attains peak force of −5300 N.

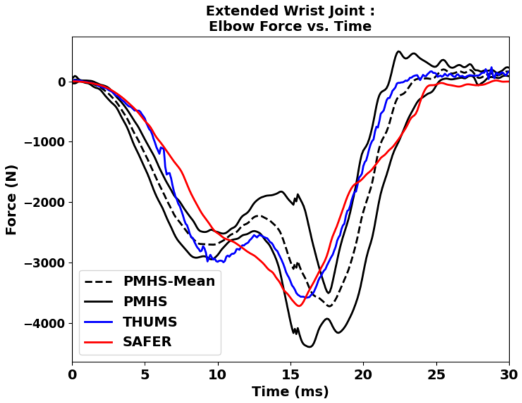

(a) Extended Wrist: Free Elbow.

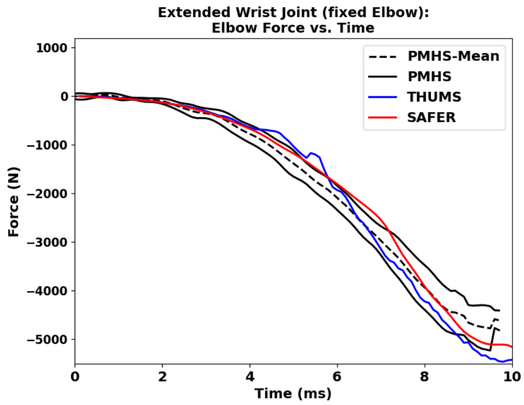

(b) Extended Wrist: Fixed Elbow.

Fig. 6. Extended wrist joint (free elbow) simulation results: elbow forces time history. THUMS M50 (blue), SAFER M50 (red), compared to the PMHS corridor (black) [19].

Condition 4: Supinated Forearm Three-point Bend Test

Figure 7 (a) shows the maximum principal strain (MPS) histories for the radius and ulna and Figure 8 (b) shows the support force time history in the supinated forearm three-point bending test. The experimental results were reported until the time of fracture.

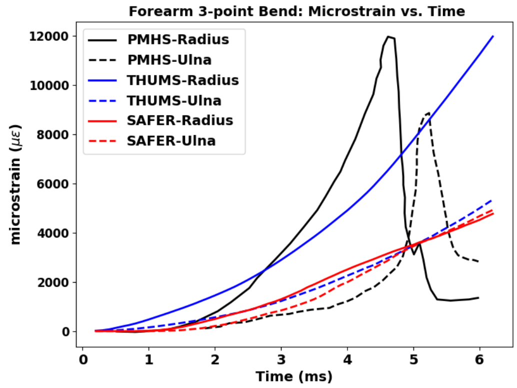

a)

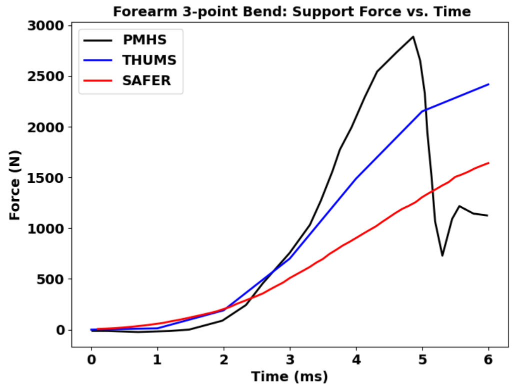

b)

Fig. 7. Forearm three-point bend simulation results: a) radius (strong line) and ulna (dotted line) microstrain time history. b) support load force time history. THUMS M50 (blue), SAFER M50 (red), compared to the mean PMHS (black).

In the supinated forearm three-point bending test, the experimental radius reached a peak MPS of approximately 12000–14000 μϵ, while the ulna peaked at around 8000 μϵ. The THUMS M50 simulation predicted higher peaks of over 120000 μϵ for the radius and approximately 5000 μϵ for the ulna. In case of SAFER M50, the peak strain was 4500 μϵ for both radius and ulna. Similarly, the support force time histories from the simulations were extracted and compared with the experimental results. The experiment showed a peak support force of approximately 2800 N at around 4.5 ms. In contrast, the simulations predicted peak forces of 2492 N for THUMS and 1608 N for SAFER, at 6 ms.

IV. DISCUSSION

Upper extremity injuries are among the most frequently observed injury types in MVCs, and accurate prediction of these injuries is critical for understanding causation mechanisms and guiding effective countermeasure design. HBMs can play an important role in injury prediction and prevention. The usefulness of HBMs depends on how well they capture the anatomy, mechanical responses, and interactions of the body region components, enabling reliable injury assessment.

This study aimed to take a preliminary look at identifying what loading cases should be targeted for biofidelity assessment of upper extremity injuries and to make an initial assessment of the current state of select upper extremity components of two widely used 50th percentile male HBMs, THUMS M50 and SAFER M50, in the defined loading conditions. The field data analysis and targeted literature review were conducted first, to identify the most frequently injured upper extremity regions, and to identify available PMHS reference data to inform HBM examination for those regions. Five loading scenarios were identified from the available PMHS data: clavicle axial compression, clavicle three-point bending, wrist compression with fixed elbow and free elbow boundary conditions, and forearm three-point bending. For each scenario, a corresponding FE model was developed that replicated the experimental boundary conditions, loading directions, and constraint definitions, enabling direct comparison with available PMHS response corridors.

Clavicle Three-point Bend and Axial Compression

In clavicle axial compression, both the THUMS M50 and SAFER M50 exhibit a stiffer response than the PMHS corridors, particularly during the early stages of loading. The HBMs quickly approach the upper corridor than observed experimentally, whereas the PMHS response increases more gradually. Following peak loading, both models display a plateau and unloading behavior that is not evident in the experimental data, which continues to sustain increasing force with deformation. Overall, the HBM responses are characterized by a more linear-plastic stiffness characteristics, whereas the experimental PMHS curves demonstrate a more hyperelastic-like response.

Under **clavicle three-point bending**, in the initial 0–3 mm impactor displacement, the THUMS M50 force-displacement response closely matches the slope and magnitude of the experimental mean and remains well within the PMHS corridors correspondence, and the SAFER M50 response falls slightly above the corridors. At larger displacements (3–5 mm), SAFER M50 tracks near the upper boundary of the experimental corridor, suggesting marginally greater stiffness relative to the mean PMHS response, while the THUMS M50 response is between mean and lower bound but remaining within the defined variability bounds. Over the full loading range, SAFER M50 exhibits peak forces approximately twice those of THUMS M50 at equivalent displacements, confirming substantially greater overall stiffness in the SAFER M50 clavicle.

Wrist Joint (Extend) Performance

For the **Extended wrist under free elbow** compression, the THUMS M50 response closely tracks the PMHS mean throughout the loading pulse, remaining well within the ±1 SD corridors and capability, capturing both the peak force magnitude (~–3500 N) and overall curve characteristics. In comparison, SAFER M50 exhibits moderately higher peak forces (~–3800 N) but remains within the upper corridor bounds. Both models accurately predict the initial rapid force rise and subsequent decay; however, SAFER M50 displays a single pronounced peak, whereas both THUMS M50 and PMHS data exhibit a characteristic double-peak response. This difference suggests potentially slight difference in wrist posture, or softer flesh around the wrist joint in SAFER M50.

Extended wrist under fixed elbow loading shows better agreement for both HBMs, with THUMS-M50 and SAFER attaining a similar peak magnitude of around −5500 N to −5700 N. Both THUMS M50 and SAFER M50 closely reproduce the overall loading characteristics and remain largely within the experimental variability throughout the simulation.

Flexed wrist – A few flexed wrist fracture (Colles' fractures) have been observed in field data, they are likely underreported due to diagnostic challenges requiring CT imaging. Here exploratory simulations were conducted to assess whether the HBM responses remained consistent or changed with wrist position. However, no PMHS data were available for the flexed wrist configuration to evaluate model biofidelity. Therefore, the simulations were performed to examine the sensitivity of model response to wrist posture and to compare trends across HBMs. The wrist of both HBMs were repositioned into flexion (Figure 8a) while keeping the forearm bones rigid to prevent artificial deformation. The same impactor setup and mean acceleration pulse derived from the extended-wrist PMHS tests were applied. Two boundary conditions were evaluated: (a) a free-elbow condition with no additional constraints and (b) a fixed-elbow condition with the elbow nodes constrained to a rigid plate, replicating the experimental setup. All other model parameters, loading conditions, and force extraction methods were kept identical to those used in the extended-wrist simulations to enable direct comparison between wrist postures.

Under free-elbow loading, flexed and extended wrist postures produced similar overall response patterns in both HBMs, characterized by an initial compressive phase followed by rebound. However, force magnitudes were consistently lower in flexion. In THUMS M50, the flexed wrist generated primary and secondary peaks of approximately −1800 N and −2200 N, compared to −3000 N and −3500 N in extension. SAFER M50 exhibited a single peak of approximately −2400 N in flexion versus −3600 N in extension.

A similar trend was observed under fixed-elbow loading, where extension produced substantially higher forces than flexion. THUMS M50 reached peak forces of approximately −4000 N in flexion and −5700 N in extension, while SAFER M50 peaked at approximately −1970 N and −5300 N, respectively. These results suggest greater joint stiffness in extension than in flexion.

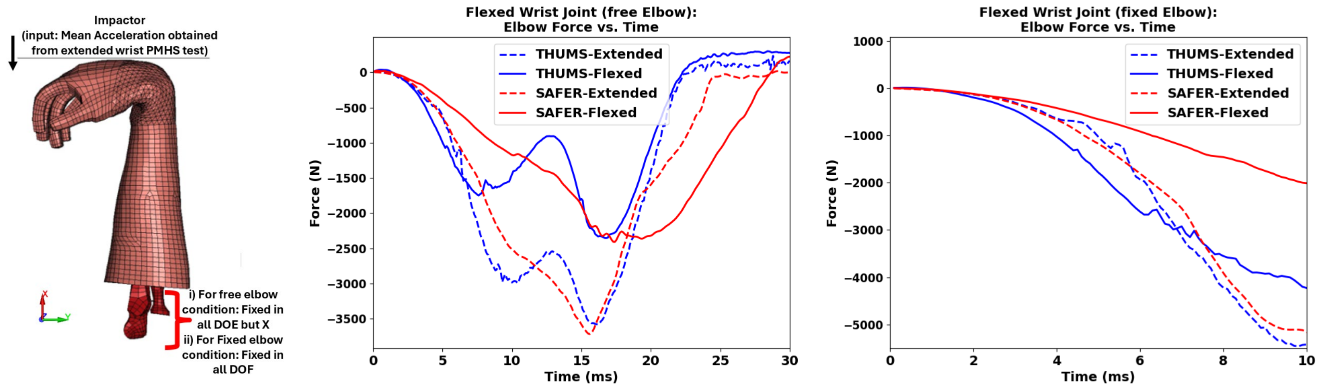

(a) Flexed Wrist Joint Axial Impact (b) Free elbow. (c) Fixed elbow.

Fig. 8. Flexed vs Extended wrist joint (a) free elbow and (b) fixed elbow simulation results: elbow forces time history. THUMS M50 (blue), SAFER M50 (red), compared to the PMHS corridor (black) [19].

No PMHS data are currently available for axial impacts to a flexed wrist, limiting assessment of model biofidelity in this configuration. Given the variability of upper-extremity postures during crashes, future PMHS studies should investigate additional wrist postures and loading modes, including axial impact to a flexed wrist, to establish injury tolerance and biofidelity reference data beyond the extended-wrist condition.

Forearm Bending Performance

The THUMS M50 and SAFER M50 simulations of the radius initially track the experimental strain response closely up to approximately 2 ms. Beyond this point, the THUMS M50 model continues to exhibit a steady increase in radial strain, exceeding 14,000 με without demonstrating the pronounced post-peak drop observed in the experimental data. Similarly, the ulna strain response is initially captured well but begins to plateau beyond approximately 4 ms, stabilizing at elevated strain levels of about 5,000 με. In contrast, the SAFER M50 model indicates comparatively lower stiffness in both the radius and ulna, with strain levels remaining around 4,200 με up to 6 ms, deviating from both the PMHS response and the THUMS predictions.

Overall Observations

Qualitatively, both models demonstrate reasonable performance in their current state relative to the available PMHS data, with similar kinematic trends, waveform shapes, and relative load partitioning as observed in the PMHS tests (including initial stiffness characteristics and the dominance of radius over ulna strains in forearm bending). However, some differences were observed. The clavicle responses tended toward greater stiffness and more gradual post-peak degradation than PMHS, and the free elbow wrist-impact condition showed reduced peak force magnitudes. Both of these suggest that further investigation may be warranted to investigate whether or not these differences substantially affect the interaction of the upper extremities with the surrounding environment, and to develop strategies for injury risk prediction in the context of these response differences. Other differences between the model responses and the PMHS results are likely attributable to a lack of deterministic representation of fracture in these simulations (for example, a lack of a drop in strain in the forearm tests with fracture). These results highlight that care is needed when interpreting model results in scenarios that may result in injury, paying attention to the potential influence that fracture modelling (or lack thereof) may have on other output measures from the model. The findings highlight the models' strengths for studying upper extremity kinematics and posture sensitivity while identifying opportunities for refinement in failure modelling and material stiffness properties of the bone such as radius and ulna to better align with experimental corridors. Such improvements will enhance HBM reliability for countermeasure development in frontal crashes and automated vehicles, where upper extremity injuries remain prominent among all occupants.

Limitations and Recommendations for Future Data Collection and Evaluation

The current study indicates that the clavicle of both HBMs showed good agreement under isolated loading conditions. While its performance within the full shoulder complex, where load transfer involves the clavicle, scapula, and surrounding tissues, should be evaluated to understand the overall biofidelity of the shoulder joint. Also, both models exhibit greater stiffness in the extended wrist posture compared to flexed. However, verification through PMHS testing is required. Notably, no PMHS data exist to date for flexed wrist compression under either fixed or free elbow conditions. Therefore, direct evaluation of HBM responses for this posture-specific loading mode could not performed. Also, forearm three-point bending validation documentation of the experimental set-up and the results remain extremely limited for both male and female. This constrains our ability to evaluate upper extremity responses and injury prediction against PMHS tests. Furthermore, both HBMs exhibited limited capability to achieve fully pronated forearm and wrist configurations. This restriction is primarily attributed to model development constraints, including geometric representation and the presence of surrounding soft tissues. Due to this limitation, the models were not evaluated for pronated three-point bend forearm load case. Finally, this study focused primarily on local, component-level comparisons. Future work should also include performing reference tests and simulations to evaluate upper extremity responses and injury prediction under system-level loading, such as whole-body frontal impact with a modern restraint system.

V. CONCLUSION

Upper extremity injuries represent one of the most frequently observed AIS2+ injury types in MVCs, often resulting from complex, multi-modal loading conditions. This study examined the current state of the upper extremity response of the THUMS-M50 and SAFER M50 HBMs at the component and joint level, under select load cases informed by injury types seen in the field. The field data analysis identified the clavicle, forearm, and wrist as the most frequently injured regions, motivating the selection of representative loading scenarios for examination. Five loading scenarios were identified from the available PMHS test literature: clavicle axial compression and three-point bending, wrist compression (fixed/free elbow), and supinated forearm three-point bending. FE simulations replicating the corresponding PMHS experimental set-ups were performed, and the resulting responses were systematically compared against available test data. Both THUMS M50 and SAFER M50 exhibited responses that were generally reasonable compared to the PMHS responses (i.e. within the same order of magnitude), though some acute differences were observed (in the stiffness responses and responses following fracture in the PMHS). Most notably, PMHS test data relating to the most frequent type of upper extremity injury – wrist fracture – are limited. Future work should include gathering additional data on wrist fracture mechanics and injury tolerance (including for males and females) to facilitate robust evaluation of HBM biofidelity and injury prediction. In addition, limitations and challenges were observed in the positioning of the models (e.g. in forearm pronation), highlighting model refinements that may be warranted to expand capabilities in upper extremity injury prediction.

VI. ACKNOWLEDGEMENTS

This work was funded by Autoliv, Sweden. The authors also acknowledge Research Computing at The University of Virginia for providing access to computational resources and technical support that have contributed to the results reported within this publication.

VII. REFERENCES

[1] Forman, J., Poplin, G. S., *et al.* (2019) Automobile injury trends in the contemporary fleet: Belted occupants in frontal collisions. *Traffic Injury Prevention*, **20**(6): pp. 607–12.
[2] Craig, M. J., Liu, C., Zhang, F., Enriquez, J. (2024) Sex-based differences in odds of motor vehicle crash injury outcomes. *Accident Analysis & Prevention*, **195**: 107100.
[3] De Putter, C. E., Selles, *et al*. (2014) Health-related quality of life after upper extremity injuries and predictors for suboptimal outcome. *Injury*, **45**(11): pp. 1752–1758.
[4] Malm, S., Krafft, M., Kullgren, A., Ydenius, A., Tingvall, C. (2008) Risk of permanent medical impairment (RPMI) in road traffic accidents. *Annals of Advances in Automotive Medicine/Annual Scientific Conference,* 52: p. 93.
[5] Kemper, A. R., McNally, C., Kennedy, E. A., Manoogian, S. J., Duma, S. M. (2008) The influence of arm position on thoracic response in side impacts. SAE Technical Paper No. 2008-22-0016.
[6] Kemper, A. R. (2013) Response corridors for the medial–lateral compressive stiffness of the human arm: Implications for side impact protection. *Accident Analysis & Prevention*, **50**: 204–222.
[6] Bolte, J. H., Hines, M. H., Herriott, R. G., McFadden, J. D., Donnelly, B. R. (2003) Shoulder impact response and injury due to lateral and oblique loading. *Stapp Car Crash Journal*, SAE Technical Paper No. 2003-22-0003.
[7] Otte, D. (1998) Biomechanics of upper limb injuries of belted car drivers and assessment of avoidance. *Proceedings of the IRCOBI Conference*, 1998, Gothenburg, Sweden.

[8 Wraighte, P. J., Manning, G., Wallace, W. A., Hynd, D. (2007) Upper extremity injuries in road traffic accidents. *Twentieth International ESV Conference*, 2007, Lyon, France, Paper No. 07-0239, 2007.
[9] Jernigan, M. V. & Duma, S. M. (2003) The effects of airbag deployment on severe upper extremity injuries in frontal automobile crashes. *The American Journal of Emergency Medicine*, **21**(2): pp. 100–105.
[10] Jernigan, M. V., Rath, A. L., Duma, S. M. (2005) Severe upper extremity injuries in frontal automobile crashes: the effects of depowered airbags. *The American Journal of Emergency Medicine*, **23**(2): pp. 99–105.
[11] Huelke, D. F., Moore, J. L., Compton, T. W., Samuels, J., Levine, R. S. (1995) Upper extremity injuries related to airbag deployments. *Journal of Trauma and Acute Care Surgery*, **38**(4): pp. 482–488.
[12] Hault-Dubrulle, A., Robache, F., *et al*. (2012) Influence of pre-crash driver posture on injury outcome: airbag interaction with human upper extremities. *Computer Methods in Biomechanics and Biomedical Engineering*, **15**(sup1): pp. 295–297.
[13] Jakobsson, L. and Lindman, M. (2010) Upper extremity fractures in car accidents. *Proceedings of the IRCOBI Conference*, 2010, Hannover, Germany.
[14] D. Hynd, J. Carroll, R. Cuerden, (2007) Upper Extremity Injury Study: Recommendations For Injury Prevention Priorities. In: Proceeding of the 20th International Technical Conference of the Enhanced Safety of Vehicles (ESV), Paper 07-0317.
[15] Wraighte, P. J., Manning, P. A., Wallace, W. A., Hynd, D. (2011) Upper Extremity Injuries in Road Traffic Accidents. *Shoulder & Elbow*, **3**(3): pp. 184–187. Jul. 2011, doi: 10.1111/j.1758-5740.2011.00107.
[16] Toyota Motor Corporation (2021) Documentation, Total Human Model for Safety, AM50 Occupant Model Version 4.1. https://www.toyota.co.jp/thums/
[17] Iraeus, J., Brynskog, E., John, J. Development of SAFER HBM v11.
[18] Zhang, Q., Kindig, M., Li, Z., Crandall, J. R., Kerrigan, J. R. (2014) Development of structural and material clavicle response corridors under axial compression and three point bending loading for clavicle finite element model validation. *Journal of Biomechanics*, **47**(11): pp. 2563–2570.
[19] Forman, J., Perry, B., *et al*. (2014) Injury tolerance of the wrist and distal forearm to impact loading onto outstretched hands. *Journal of Trauma and Acute Care Surgery*, **77**(3): pp. S176–183.
[20] Duma, S. M., Schreiber, P. H., McMaster, J. D., Crandall, J. R., Bass, C. R. (2002a) Fracture tolerance of the male forearm: the effect of pronation versus supination. *Proceedings of the Institution of Mechanical Engineers, Part D: Journal of Automobile Engineering*, **216**(8): pp. 649–654.